

# The Relevance of Mediterranean Neutrino Telescope Sites on Earth-skimming tau neutrino detection

G. Miele<sup>a\*</sup>

<sup>a</sup>Dipartimento di Scienze Fisiche, Università di Napoli *Federico II* and INFN Sezione di Napoli, Complesso Universitario di Monte S. Angelo, Via Cinthia, I-80126 Napoli, Italy.

A study of the UHE  $\nu_\tau$  detection performances of a  $\text{km}^3$  Neutrino Telescope sitting at the three proposed sites for ANTARES, NEMO and NESTOR in the Mediterranean sea is here performed. In particular, it is analyzed the effect of the underwater surface profile on the total amount of yearly expected  $\tau$  crossing the fiducial volume in the limit of full detection efficiency and energy resolution.

## 1. Introduction

Neutrinos are one of the main components of the cosmic radiation in the ultra-high energy (UHE) regime. Although their fluxes are uncertain and depend on the production mechanism, their detection can provide information on the sources and origin of the UHE cosmic rays. For example, UHE neutrinos can be produced via  $\pi$ -photoproduction by strongly accelerated hadrons in presence of a background electromagnetic field. This scenario is expected to occur in extreme astrophysical environments like the jets of active galactic nuclei, radio galaxies and gamma ray burst sources as well as in the propagation of UHE nucleons scattering off the cosmic background radiation (known as *cosmogenic neutrinos* [1,2]).

From the experimental point of view, after the first pioneering and successful achievements neutrino astronomy in the high energy regime [3,4,5,6,7] is a rapidly developing field, with a new generation of neutrino telescopes on the way, as in the deep water of the Mediterranean sea, namely ANTARES [8], NESTOR [9] and NEMO [10]. In the future they could lead to the construction of a  $\text{km}^3$  telescope as pursued by the KM3NeT project [11,12].

Although NTs were originally thought as  $\nu_\mu$  detectors, their capability as  $\nu_\tau$  detectors has become a hot topic [13,14,15,16], in view of the

fact that flavor neutrino oscillations lead to nearly equal astrophysical fluxes for the three neutrino flavors. Despite the different behavior of the produced tau leptons with respect to muons in terms of energy loss and decay length, both  $\nu_\mu$  and  $\nu_\tau$  detection are sensitive to the matter distribution near the NT site [17]. Thus, a computation of the event detection rate of a  $\text{km}^3$  telescope requires a careful analysis of the surroundings of the proposed site. The importance of the elevation profile of the Earth surface around the detector was already found of some relevance in Ref. [18,19], where the present author and others calculated the aperture of the Pierre Auger Observatory [20,21] for Earth-skimming UHE  $\nu_\tau$ 's.

In this paper it is computed the effective aperture for  $\nu_\tau$  detection of a  $\text{km}^3$  NT in the Mediterranean sea placed at any of the three locations proposed by the ANTARES, NEMO and NESTOR collaborations. A more complete treatment of the subject also including the  $\nu_\mu$  contribution is contained in Ref. [17].

A detailed DEM of the under-water Earth surface is available from the Global Relief Data survey (ETOPO2) [22], a grid of altimetry measurements with a vertical resolution of 1 m averaged over cells of 2 minutes of latitude and longitude. In Figures 1, 2 and 3 are shown the 3D maps of the areas around the three NT sites. The black curve represents the coast line, whereas the red spot stands for the location of the apparatus. By

\*electronic address: miele@na.infn.it

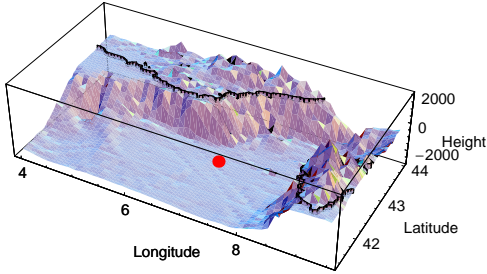


Figure 1. The surface profile of the area near the ANTARES site (red spot) at  $42^\circ 30' \text{ N}$ ,  $07^\circ 00' \text{ E}$ . The black curve represents the coast line. The sea plateau depth in the simulation is assumed to be 2685 m.

following the same approach developed in [18], this DEM is used to produce a realistic and statistically significant sample of  $\nu_\tau/\tau$  tracks crossing the fiducial volume of the NT that are then used to evaluate the effective aperture of each detector.

The structure of the paper is as follows. In Section 2 the formalism and definitions used in the analysis are introduced, and the aperture for a NT is defined. The results for  $\nu_\tau$  induced events are reported and discussed in Section 3 for various incoming neutrino fluxes. Finally, the conclusions are reported in Section 4.

## 2. The effective aperture of a NT

Let us define the  $\text{km}^3$  NT *fiducial* volume as that bounded by the six lateral surfaces  $\Sigma_a$  (the subindex  $a=W, E, N, S, U$  and  $D$  labels each surface through its orientation: West, East, North, South, Up, and Down), and indicate with  $\Omega_a \equiv (\theta_a, \phi_a)$  the generic direction of a track entering the surface  $\Sigma_a$ . The scheme of the NT fiducial volume and two examples of incoming tracks are shown in Fig. 4.

Let  $d\Phi_\nu/(dE_\nu d\Omega_a)$  be the differential flux of UHE  $\nu_\tau + \bar{\nu}_\tau$ . The number per unit time of  $\tau$

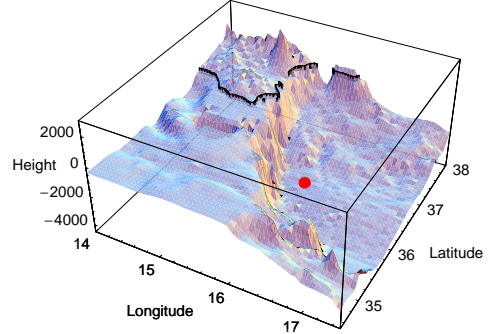


Figure 2. The surface profile of the area near the NEMO site (red spot) at  $36^\circ 21' \text{ N}$ ,  $16^\circ 10' \text{ E}$ . The black curve represents the coast line. The sea plateau depth used in the simulation is 3424 m.

leptons emerging from the Earth surface and entering the NT through  $\Sigma_a$  with energy  $E_\tau$  is given by

$$\left(\frac{dN_\tau}{dt}\right)_a = \int d\Omega_a \int dS_a \int dE_\nu \frac{d\Phi_\nu(E_\nu, \Omega_a)}{dE_\nu d\Omega_a} \times \int dE_\tau \cos(\theta_a) k_a^\tau(E_\nu, E_\tau; \vec{r}_a, \Omega_a). \quad (1)$$

This equation is the same as that in [18], but for full duty cycle and detection efficiency. The kernel  $k_a^\tau(E_\nu, E_\tau; \vec{r}_a, \Omega_a)$  is the probability that an incoming  $\nu_\tau$  crossing the Earth, with energy  $E_\nu$  and direction  $\Omega_a$ , produces a  $\tau$ -lepton which enters the NT fiducial volume through the lateral surface  $dS_a$  at the position  $\vec{r}_a$  with energy  $E_\tau$  (see Fig. 4 for the angle definition). If one splits the possible events between those with track intersecting the *rock* and the ones only crossing *water*, the kernel  $k_a^\tau(E_\nu, E_\tau; \vec{r}_a, \Omega_a)$  is given by the sum of these two mutually exclusive contributions,

$$k_a^\tau(E_\nu, E_\tau; \vec{r}_a, \Omega_a) = k_a^{\tau,r}(E_\nu, E_\tau; \vec{r}_a, \Omega_a) + k_a^{\tau,w}(E_\nu, E_\tau; \vec{r}_a, \Omega_a). \quad (2)$$

For an isotropic flux one can rewrite Eq. (1), summing over all the surfaces, as

$$\frac{dN_\tau^{(r,w)}}{dt} = \int dE_\nu \frac{1}{4\pi} \frac{d\Phi_\nu(E_\nu)}{dE_\nu} A^{\tau(r,w)}(E_\nu)$$

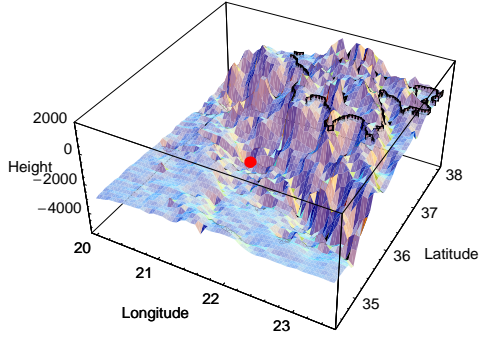


Figure 3. The surface profile of the area near the NESTOR site (red spot) at  $36^\circ 21' \text{ N}$ ,  $21^\circ 21' \text{ E}$ . The black curve represents the coast line. The sea plateau depth in the simulation is assumed to be 4166 m.

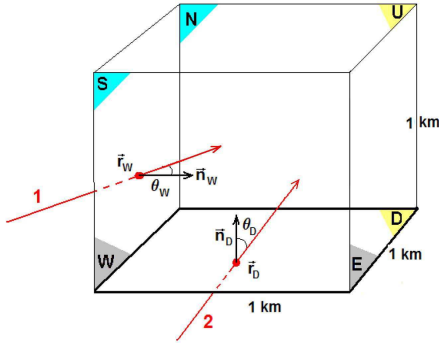


Figure 4. The angle definition and the fiducial volume of a  $\text{km}^3$  NT.

$$= \sum_a \int dE_\nu \frac{1}{4\pi} \frac{d\Phi_\nu(E_\nu)}{dE_\nu} A_a^{\tau(r,w)}(E_\nu), \quad (3)$$

which defines the total aperture  $A^{\tau(r,w)}(E_\nu)$ , with "r" and "w" denoting the *rock* and *water* kind of events, respectively. The contribution of each surface to the total aperture reads

$$A_a^{\tau(r,w)}(E_\nu) = \int dE_\tau \int d\Omega_a \int dS_a \cos(\theta_a) \times k_a^{\tau,(r,w)}(E_\nu, E_\tau; \vec{r}_a, \Omega_a). \quad (4)$$

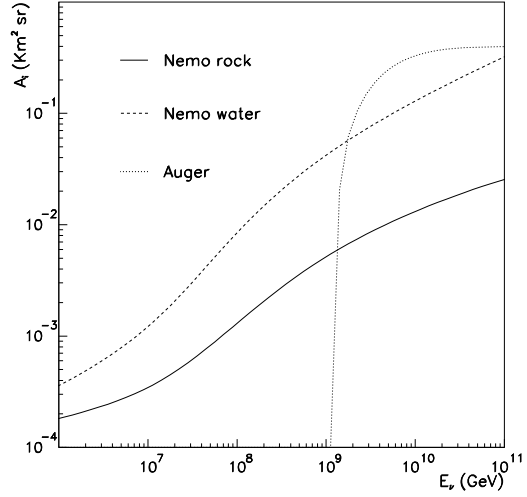


Figure 5. The effective apertures  $A^{\tau(r)}(E_\nu)$  (solid line) and  $A^{\tau(w)}(E_\nu)$  (dashed line) defined in Eq. (3) versus neutrino energy for NEMO. The dotted line corresponds to the same quantity for the Auger Fluorescence Detector for Earth-skimming  $\nu_\tau$  as in [18].

### 3. The event rate for $\nu_\tau$ interactions

In Fig. 5 are shown the apertures  $A^{\tau(r,w)}$  for the NEMO site together with the corresponding quantity for the Pierre Auger Observatory Fluorescence Detector (FD) calculated in [18]. Note that the Auger case is only for Earth-skimming  $\tau$ 's, since down-going neutrino induced events can be disentangled from ordinary cosmic rays only for very inclined showers. Interestingly, the NEMO-*water* and Auger-FD apertures almost match at the FD threshold of  $10^{18}$  eV, so that using both detectors results into a wide energy range of sensitivity to  $\nu_\tau$  fluxes.

In Fig. 6 we show the high energy behavior for each surface contributing to the effective aperture. For *rock* events there is a clear W-E asymmetry, easily understood in terms of matter effects related to the particular morphology of the NEMO site (see Fig. 2). A much smaller S-N asymmetry is also present. For neutrino energies larger than  $10^7$  GeV the main contribution

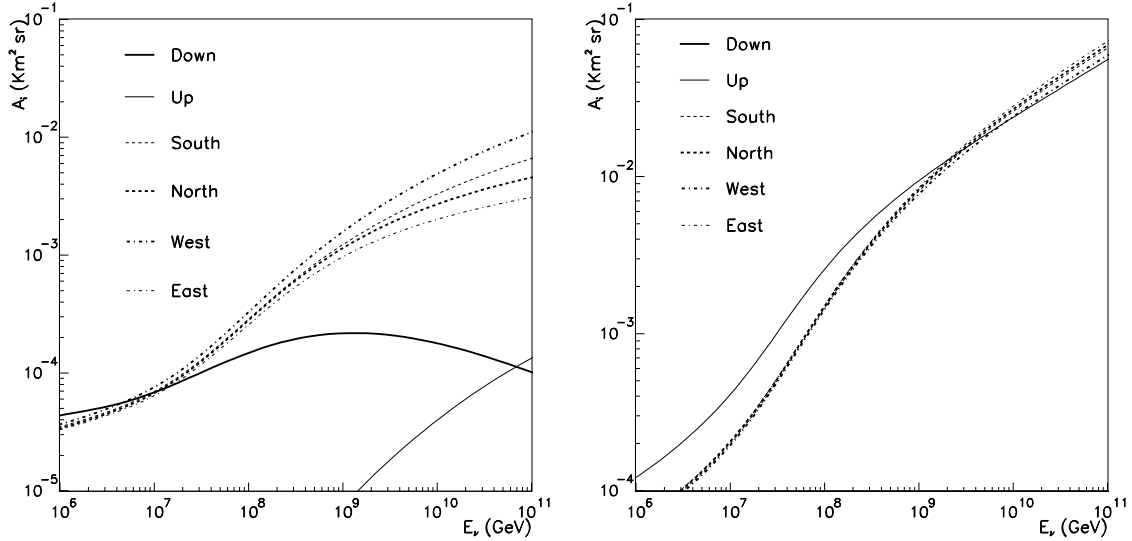


Figure 6. The effective apertures  $A_a^{\tau(r,w)}(E_\nu)$  of Eq. (4) versus neutrino energy for (left) *rock* events and (right) *water* events for the NEMO site.

to the aperture  $A^{\tau(r)}(E_\nu)$  comes from the lateral surfaces, i.e. from  $\tau$  leptons emerging from the rock far from the NT basis and crossing the fiducial volume almost horizontally. Instead, the upper surface contribution is negligible due to the very small fraction of events crossing the rock and entering the detector from above. For *water* events the contribution to the aperture from all surfaces is comparable (except for the lower one which has no events), the upper one providing a slightly larger contribution as the energy decreases. Indeed, events which would cross the lateral surfaces should travel over a longer path in water and this becomes more unlikely at lower energies due to the shorter  $\tau$  decay length.

In Fig. 7 the detection performances of a km<sup>3</sup> NT placed at one of the three sites in the Mediterranean sea are compared. In particular the quantities

$$\frac{[A^{\tau((r,w))}(\text{NESTOR}) - A^{\tau((r,w))}(\text{NEMO})]}{A^{\tau((r,w))}(\text{NEMO})}$$

$$\frac{[A^{\tau((r,w))}(\text{ANTARES}) - A^{\tau((r,w))}(\text{NEMO})]}{A^{\tau((r,w))}(\text{NEMO})} \quad (5)$$

are plotted versus the neutrino energy.

The NESTOR site shows the highest values of

the  $\tau$ -aperture for both *rock* and *water*, due to its larger depth and the particular matter distribution of the surrounding area, while the lowest rates are obtained for ANTARES. The aperture in the three sites can be quite different at high energy but the net effect of this on the expected number of events per year is not particularly significant since the UHE neutrino flux drops rapidly with the energy.

Knowing the aperture of the NT at each site, one can compute the expected  $\tau$  event rate, once a neutrino flux is specified. In Table 1 these rates are shown assuming a GZK-WB flux. The enhancement effect due to the local matter distribution is responsible for the N-S, W-E and NE-SW asymmetries for the ANTARES, NEMO and NESTOR sites, respectively, as expected from the matter profiles shown in Figs. 1, 2 and 3. These matter effects, for the specific UHE flux considered (GZK-WB), correspond to an enhancement of *rock* events of the order of 20% and a screening factor for *water* events of the order of a few percent. This is easily understood since for *water* events the U surface gives a significant contribution which is essentially unaffected by matter distribution.

Surf.	ANTARES	NEMO	NESTOR
D	0.0086/0	0.0086/0	0.0085/0
U	0/0.1741	0.0002/0.2191	0.0003/0.2595
S	0.0219/0.1635	0.0290/0.1799	0.0287/0.2014
N	0.0275/0.1573	0.0268/0.1847	0.0359/0.1938
W	0.0247/0.1616	0.0371/0.1715	0.0303/0.2020
E	0.0240/0.1622	0.0228/0.1900	0.0414/0.1858
Total	0.107/0.819	0.124/0.945	0.145/1.043

Table 1

Estimated rate per year of *rock/water*  $\tau$  events at the three  $\text{km}^3$  NT sites for a GZK-WB flux. The contribution of each detector surface to the total number of events is also reported.

It is important to emphasize that the role of matter effects depends critically upon the energy spectrum of the UHE neutrino flux. For more energetic neutrino fluxes the enhancement factor is expected to be more significant (see the energy behavior of  $A_a^{\tau(r)}(E_\nu)$  in Fig 6).

In Table 2 the rate of *rock/water*  $\tau$  events are computed for the three different  $\text{km}^3$  NT sites using several UHE neutrino fluxes as already considered in [18,23] and described in [24]-[30]. As can be seen from Table 2, the enhancement factors due to matter effects on *rock* events can be as large as 30%, whereas the difference in the rates of *water* events for a fixed neutrino flux is mainly due to the different depth of the three sites.

An interesting feature is the dependence of the event rate upon the shape of the NT detector for a fixed total volume of  $1 \text{ km}^3$ , a property that might be relevant for the eventual design of the detector. Consider for example a  $\text{km}^3$  NT placed at the NEMO site with the shape of a parallelepiped rather than a cube, where in particular the E and W surfaces are enlarged by a factor 3 in the horizontal dimension, the N and S surfaces being reduced by the same factor, keeping the height of towers still of 1 km. In this case the expected rate of *rock* events per year is enhanced by almost a factor 2, from 0.12 to 0.21 for the GZK-WB flux, while this enhancement could be even larger for neutrino fluxes with a larger high energy component. Moreover, the expected rate of *water* events increases as well by a factor of the order of 50%, from 0.945 up to 1.425 per year. Similar exercises can be also performed for the ANTARES

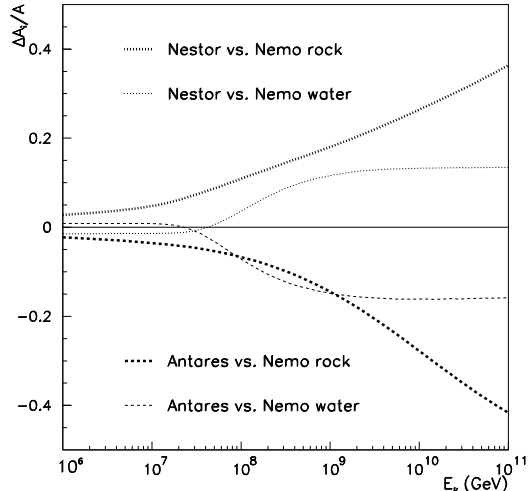


Figure 7. A comparison of the effective NT apertures with respect to the NEMO one is shown versus the neutrino energy (see Eq. 5 for definitions).

and NESTOR sites. Of course, a further possibility which might favor UHE- $\tau$  detection consists in increasing the effective volume of the detector keeping unchanged the 1 km height and the number of towers of photomultipliers but adopting a larger spacing. As an example, for a factor four larger volume with a doubling of the tower spacing both the *rock* and *water*  $\tau$  events would increase by almost a factor two, but obviously at the expense of the energy threshold and the quality of the event reconstruction for “low-energy” (TeV) neutrinos. For a detector aiming at the exploration of the range above the PeV, this is a less severe problem.

The fact that the event rate depends upon the total surface of the detector is a peculiar feature of a NT, quite differently from what expected at the Auger observatory. Actually, in this case observed showers are generally initiated not very far from the detector compared to its dimensions so that the shape of the detector (i.e., the position on the border where the FDs are placed) is not as important as its “volume” (controlled by the area enclosed by the FDs). In fact, in order to produce a  $\tau$  emerging from the Earth with

$\nu$ -fluxes	ANTARES	NEMO	NESTOR
GZK-WB	0.107/0.819	0.124/0.945	0.145/1.043
GZK-L	0.110/1.106	0.141/1.308	0.175/1.471
GZK-H	0.245/2.284	0.335/3.348	0.423/3.777
NH	1.029/8.920	1.248/10.37	1.488/11.51
TD	0.837/5.181	0.957/5.888	1.087/6.436

Table 2

Yearly rate of *rock/water*  $\tau$  events at the three  $\text{km}^3$  NT sites for different UHE neutrino fluxes. GZK-H is for an initial proton flux  $\propto 1/E$ , assuming that the EGRET flux is entirely due to  $\pi$ - photoproduction. GZK-L shows the neutrino flux when the associated photons contribute only up to 20% in the EGRET flux. GZK-WB stands for an initial proton flux  $\propto 1/E^2$  [24]–[28]. The other two neutrino fluxes correspond to more exotic UHECR models. NH represents the neutrino flux prediction in a model with new hadrons [29], whereas TD is the neutrino flux for a topological defect model [30].

enough energy to generate a shower detectable by the Auger FDs (at least 1 EeV =  $10^{18}$  eV), the energy of the neutrino should be larger than  $10^{18}$  eV, taking into account the  $\tau$  energy loss in the rock. But the decay length of such a UHE  $\tau$  is  $l_{\text{decay}} \simeq 50 \text{ km} \times (E_{\tau}/\text{EeV})$ , to be compared with the dimensions of the Auger fiducial volume,  $\sim 50 \times 60 \times 10 \text{ km}^3$ . Conversely, a neutrino telescope can detect tau’s or muons which are produced very far from the detector by a neutrino charged-current interaction, from distances comparable to the charged lepton range at that particular energy [16]. Indeed, the  $\tau$  range in water is of the order of several kilometers: from the value of  $\beta_{\tau} = 0.71 \times 10^{-6} \text{ cm}^2 \text{ g}^{-1}$  one obtains an attenuation length  $1/(\beta_{\tau} \rho_w) \simeq 15 \text{ km}$ , while for muons (see [17]) the range is approximately eight times smaller, of the order of 2 km. In other words, the effective volume of a NT of the kind discussed so far can be much larger than  $1 \text{ km}^3$ , thus maximizing the detector area might greatly improve the detection rate.

Of course, one should not forget that the design of a NT also depends strongly upon more detailed experimental considerations. Shapes which are not very compact or a detector with very

sparse instrumentation have worse performances in the reconstruction of track properties as well as in signal-background separation, though this is mainly problematic at energies lower than 100 TeV, in the atmospheric neutrino energy range. In any case, the present analysis suggests that the choice of the detector shape could be an important feature in orienting the target of a NT investigation towards either atmospheric or extra-atmospheric neutrino physics. In this respect, the possibility to modify this parameter quite easily for a NT water detector offers a great advantage with respect to an under-ice detector.

One of the main motivations for studying UHE neutrinos is that they provide a possibility to explore a range of energies for scattering processes which is still untested (maybe impossible to test) by particle accelerators. In this respect, measuring the neutrino–nucleon cross sections at high energies could have a large impact on constraining or discovering new physics beyond the standard model (see e.g. [15,31]). While a measurement of the event energy spectrum cannot remove in general a degeneracy between the neutrino cross section and the incoming neutrino flux, a neutrino telescope could offer the interesting capability of disentangling these two factors because of the role of matter effects. Indeed, provided that enough statistics is collected and the detector has a good zenith angle resolution, the flux dependence can be subtracted off by measuring the ratio of the event rates coming from different directions [32,33,34]. In the left panel of Fig. 8 we show how the NEMO effective apertures for  $\tau$  *rock* and *water* events change if the neutrino-nucleon cross section is half or twice the standard model result while in the right panel we display the ratio of *water/rock*  $\tau$  event rates for several adopted fluxes. One can see that this ratio is quite sensitive to the value of the cross section. In particular, the number of *rock* events is essentially unaffected while the *water* event rate increases almost linearly with the cross section. Clearly, since the statistical error on the ratio would be dominated by the rare *rock* events, an experiment which aims at exploiting this effect should maximize the acceptance for almost horizontal events. It is important noticing that the present results

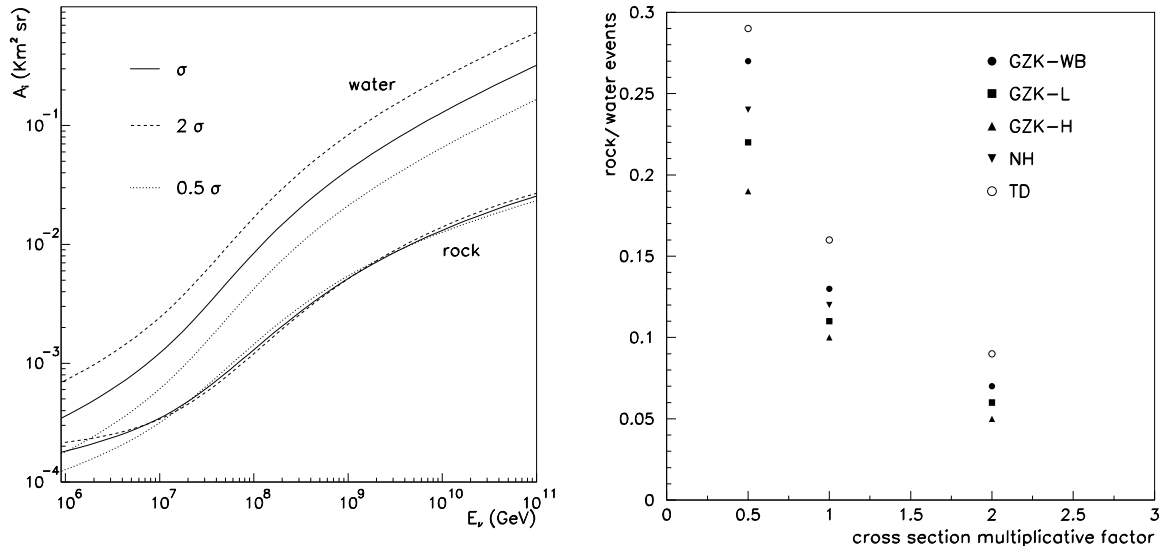


Figure 8. (Left) The effective apertures  $A^{\tau(r,w)}(E_\nu)$  for the NEMO site for a  $\nu_\tau$ -nucleon cross section multiplied by a factor 0.5, 1 and 2 with respect to the standard result  $\sigma$ . (Right) Ratios of the number of events in *rock/water* when the cross section is rescaled by the factor shown on the  $x$  axis, for several incoming UHE neutrino fluxes.

do not take into account any detailed experimental setup and up to this point the  $\nu_\mu$  contribution is not yet considered. Nevertheless, since both the incoming neutrino flux and cross section on nucleons are expected to be flavor independent the possibility of determining both these quantities at a NT seems an interesting perspective.

#### 4. Conclusions

Ultra-high energy neutrinos represent one of the main targets for several experiments which adopt a variety of detection techniques. Among these, the optical Cherenkov neutrino telescopes, deployed under water or ice, look for the tracks of charged leptons produced by the high energy neutrinos that reach the Earth. In this paper, it has been presented a new study of the performance of a  $\text{km}^3$  neutrino telescope to be located in any of the three sites in the Mediterranean sea proposed by the ANTARES, NEMO, and NESTOR collaborations. In particular the details of the under-water surface profile of each of the three sites, using the data from a Digital Elevation Map, have been

considered. By generating a realistic and statistically significant sample of  $\nu_\tau/\tau$  tracks crossing the fiducial volume of the  $\text{km}^3$  neutrino telescope, the effective aperture to UHE  $\nu_\tau$  neutrinos have been calculated, as well as the expected number of events for different UHE neutrino fluxes, for both cases where the charged lepton is produced in rock and water near the telescope site.

Although in the present paper the detector-specific features, like partial detection efficiency and finite energy resolution, have not included, the obtained results show that the impact of the site geography (or matter effects) on observables such as the total event rate or asymmetries in the event direction can be important.

These matter effects can be enhanced by a suitable choice of the geometry of the telescope with a fixed volume. We have also briefly discussed the possibility of obtaining information on both the neutrino flux and the neutrino-nucleon cross section in the UHE range by measuring the ratio of rock and water events.

## REFERENCES

1. V.S. Berezinsky and G.T. Zatsepin, *Phys. Lett. B* **28** (1969) 423.
2. V.S. Berezinsky and G.T. Zatsepin, *Sov. J. Nucl. Phys.* **11** (1970) 111 (1970 *Yad. Fiz.* **11** 200).
3. T.K. Gaisser, F. Halzen and T. Stanev, *Phys. Rep.* **258** (1995) 173.
4. J.G. Learned and K. Mannheim, *Ann. Rev. Nucl. Part. Sci.* **50** (2000) 679.
5. C. Spiering, *Prog. Particle Nucl. Phys.* **48** (2002) 43.
6. F. Halzen and D. Hooper, *Rept. Prog. Phys.* **65** (2002) 1025.
7. A.B. McDonald et al., *Rev. Sci. Instrum.* **75** (2004) 293.
8. E. Aslanides et al., astro-ph/9907432.
9. S. Bottai, Contribution to 26th ICRC, Salt Lake City, AIP Conf. Proc. **516** vol 2 (1999) 456.
10. G. Riccobene, Proc. of the Workshop on Methodical Aspects of Underwater/Ice Neutrino Telescopes, 61 (2002)
11. U.F. Katz, *Prog. Part. Nucl. Phys.* **57** (2006) 273.
12. U.F. Katz, astro-ph/0606068.
13. S.I. Dutta, M.H. Reno and I. Sarcevic I, *Phys. Rev. D* **62** (2000) 123001.
14. M.C. González-García, F. Halzen and M. Maltoni, *Phys. Rev. D* **71** (2005) 093010.
15. L. Anchordoqui and F. Halzen, hep-ph/0510389.
16. S. Yoshida, R. Ishibashi and H. Miyamoto, *Phys. Rev. D* **69** (2004) 103004.
17. A. Cuoco, G. Mangano, G. Miele, S. Pastor, L. Perrone, O. Pisanti and P. D. Serpico, astro-ph/0609241.
18. G. Miele, S. Pastor and O. Pisanti, *Phys. Lett. B* **634** (2006) 137.
19. G. Miele, L. Perrone and O. Pisanti, *Nucl. Phys. Proc. Suppl.* **145** (2005) 347.
20. Pierre Auger Collaboration, 1996 *The Pierre Auger Project Design Report*, FERMILAB-PUB-96-024.
21. J. Abraham et al. (Pierre Auger Collaboration), *Nucl. Instrum. Meth. A* **523** (2004) 50.
22. U.S. Department of Commerce, National Oceanic and Atmospheric Administration, National Geophysical Data Center, 2001 *2-minute Gridded Global Relief Data (ETOPO2)*, <http://www.ngdc.noaa.gov/mgg/fliers/01mgg04.html>
23. C. Aramo et al., *Astropart. Phys.* **23** (2005) 65.
24. E. Waxman and J.N. Bahcall, *Phys. Rev. D* **59** (1999) 023002.
25. O.E. Kalashev, V.A. Kuzmin and D.V. Semikoz, astro-ph/9911035.
26. O.E. Kalashev, V.A. Kuzmin and D.V. Semikoz, *Mod. Phys. Lett. A* **16** (2001) 2505.
27. O.E. Kalashev et al., *Phys. Rev. D* **66** (2002) 063004.
28. D.V. Semikoz and G. Sigl, *JCAP* **0404** (2004) 003.
29. M. Kachelriess, D.V. Semikoz and M.A. Tórtola, *Phys. Rev. D* **68** (2003) 043005.
30. P. Bhattacharjee and G. Sigl, *Phys. Rep.* **327** (2000) 109.
31. L.A. Anchordoqui et al., *Phys. Rev. D* **72** (2005) 065019.
32. A. Kusenko A and T.J. Weiler, *Phys. Rev. Lett.* **88** (2002) 161101.
33. D. Hooper, *Phys. Rev. D* **65** (2002) 097303.
34. S. Hussain et al., hep-ph/0606246.